Desalination and Water Treatment
www.deswater.com
33 (2011) 22–35
September
1944-3994 / 1944-3986 © 2011 Desalination Publications. All rights reserved.
doi: 10.5004/dwt.2011.2627

Modeling the Nestos River plume dynamics using ELCOM

N. Kamidis[a,b]*, G. Sylaios[a], V.A. Tsihrintzis[a]

[a]*Laboratory of Ecological Engineering & Technology, Department of Environmental Engineering, Democritus University of Thrace, 67100 Xanthi, Greece*
Tel. +30 2594022691-3; Fax +30 2594022222; email: nikkami@inale.gr
[b]*National Agricultural Research Foundation, Fisheries Research Institute, Nea Peramos, 64007, Kavala, Greece*

Received 10 February 2010; Accepted in revised form 5 November 2010

ABSTRACT

Results from the first attempt to simulate the Nestos River plume using the three-dimensional numerical model ELCOM are presented. The numerical model was validated using in-situ CTD data from three field campaigns taking place under variable discharge and meteorologic conditions. Results showed that the model predicted satisfactorily the surface expansion and the shape of Nestos river plume in all cases. The calculated versus observed salinity values showed significant correlations under high, moderate-high and low flow condition. The numerical model revealed that Nestos plume enters the Kavala Gulf only under high and intermediate river flow conditions, and only under favorable east and northeast winds. After validation, the model was used to examine plume behavior under four test cases of variable discharge and winds. These results illustrated that Nestos plume is mostly wind-driven, while river discharge is the key parameter responsible for transporting the plume away from the mouth. The plume directed mainly westwards throughout the year, under the influence of the general water circulation and the predominance of E–NE winds. Local coastal morphology such as the existence of the Thassos Passage also plays a significant role on the plume dispersion and movement.

Keywords: River plume; Coastal zone; Numerical model; ELCOM; Nestos River; Kavala Gulf

1. Introduction

River discharge plays an important role on the hydrodynamics, biogeochemistry, productivity and the dynamic stability of coastal environments [1]. In terms of hydrodynamics, the introduction of river freshwater induces fresh-to-salt water frontal zones, with the buoyant freshwater spreading away from the river mouth in the form of a surface river plume [2]. The motion of the plume appears generally influenced by external forcing of larger temporal and spatial scales, as the ambient coastal circulation, the latitude-dependent deflective Coriolis force, the wind stress and the tidal variability [3]. In terms of biogeochemistry, river plume water transports organic and inorganic, dissolved and particulate nutrient compounds of nitrogen, phosphorus and carbon, thereby altering the cycling of these elements in the coastal zone [4]. As the rate of nutrient loads through rivers has risen, due to the impact of point or non-point pollution sources, more frequent and more toxic eutrophication incidents

* Corresponding author.

Presented at the 2nd International Conference on Environmental Management, Engineering, Planning and Economics (CEMEPE), Mykonos, Greece, June 21–26, 2009.

occur in the coastal marine environments [5–7]. However, this enhancement of surface biological production may produce limitations in bottom light penetration and dissolved oxygen exhaustion, thus hampering benthic primary production [8,9]. Increased nutrients and plankton levels favour the development of nursery grounds, attracting juveniles from any fish species, whose survival and growth at these early stages depend strongly on plume water dispersal and expansion [10]. In parallel, fluvial suspended particulate matter (SPM) contained within plume water, contribute into coastal sedimentation, regulate the optical characteristics of the water column and play a major role in the transport and dispersion of trace metals in estuarine and coastal environments [11]. Finally, buoyancy inputs enhance water column stability through density stratification and alter the vertical distribution of physical and chemical water properties [12].

It occurs from the above that river plumes are relevant actors in shaping and supporting various aspects of the socio-economic environment in areas close to river mouths [13]. However, river plume characteristics are also prone to hydrological alterations that often take place along a river catchment by various human interventions. The impounding of freshwater behind dams regulates discharge downstream, causing significant reductions and alterations in the timing, magnitude and frequency of high and low river flows, ultimately producing a hydrologic regime significantly different from the pre-damming natural flow regime [14,15]. Under these conditions, especially in the arid and micro-tidal Mediterranean environment, the freshwater flux and the local winds appear as the most important factors determining river plume dynamics. The complexity of interaction between meteorological and hydrodynamic features, freshwater input and coastal morphology, together with human alterations, make numerical modeling an important tool, useful in understanding the processes governing horizontal plume spreading and vertical mixing.

Under the above conditions, understanding the mechanisms responsible for the spreading and dispersion of Nestos River plume along the Thracian Sea coastal zone is of particular importance for coastal environmental processes, especially as Nestos River plume dynamics have never been studied previously. In this work, results on the spatial and temporal variability of Nestos River buoyant spreading are shown, based on a field monitoring program and the application of a three-dimensional numerical hydrodynamic model. The study is focused primarily on the freshwater mass transport within the area of interest, attempting to describe the mechanisms responsible for this transport. Collected field data were used to validate model results. After validation, the investigation of Nestos River plume behavior was studied under four typical cases of variable river discharge and wind conditions.

2. Materials and methods

2.1. Study area

2.1.1. Nestos River description

The Nestos/Mesta River is one of the 71 internationally shared river catchments of Europe [16], having its source in Rila Mountains (southwestern Bulgaria), draining an area of 5,613 km², of which 2,768 km² (or 49.34% of the total basin) belong to Bulgaria, entering Greece a few kilometers upstream of Thissavros Reservoir and turning into river downstream of Platanovrisi Reservoir, crossing the Gorges and the Delta area, until its final outflow in the Thracian Sea [17]. The relief in the whole drainage basin is mountainous and semi-mountainous, apart from the Delta area where a floodplain is formed covering 440 km². Agriculture is the leading economic sector in Nestos River Basin, while production of energy, industry and tourism are also important economic activities [18]. A third dam at Toxotes serves an extensive irrigation network for 131 km² arable land at the deltaic zone (Fig. 1).

The mean pre-damming annual discharge at the site Temenos during the period 1966–1996 was 39.7 m³/s, characterized by a strong seasonal and inter-decadal variability (data from Public Electricity Cooperation). This reduction coincided with the period of dam construction at Thissavros and Platanovrisi (1986–1997). During dam operation, freshwater runoff depicted a slight increase to 828×10^6 m³ per year, with limited seasonal variability throughout the whole year [19,20].

2.1.2. Coastal zone description

The Nestos River outflows its freshwater on an almost East-West oriented coastline, between Kavala and Vistonikos Gulf (Fig. 1). The area is shallow with gradual depth increase, reaching 50 m depth approximately 20 km southwards of the Nestos River mouth. The coastal flow is influenced by the presence of the Thassos Island to the southwest of the river mouth, showing higher velocities at the Thassos Passage and before the Kavala Gulf entry (Fig. 1). This flow comprises the Black Sea Water (BSW), discharged through the Dardanelles Strait, moving cyclonically along the Thracian Sea coastline [21,22] and entering the Kavala Gulf through the Thassos Passage [23]. BSW occupies the first 40 m of the water column, overtopping the more saline and warmer Levantine Intermediate Water (LIW) [24].

2.2. Monitoring program

2.2.1. Nestos River discharge monitoring

Twenty one field campaigns were carried out at 4 stations throughout the year 2006, along the downstream part of Nestos (Fig. 2). Furthermore, river discharge was measured through an auto-recording telemetric station, located 20 km upstream of the river mouth (Fig. 2). The

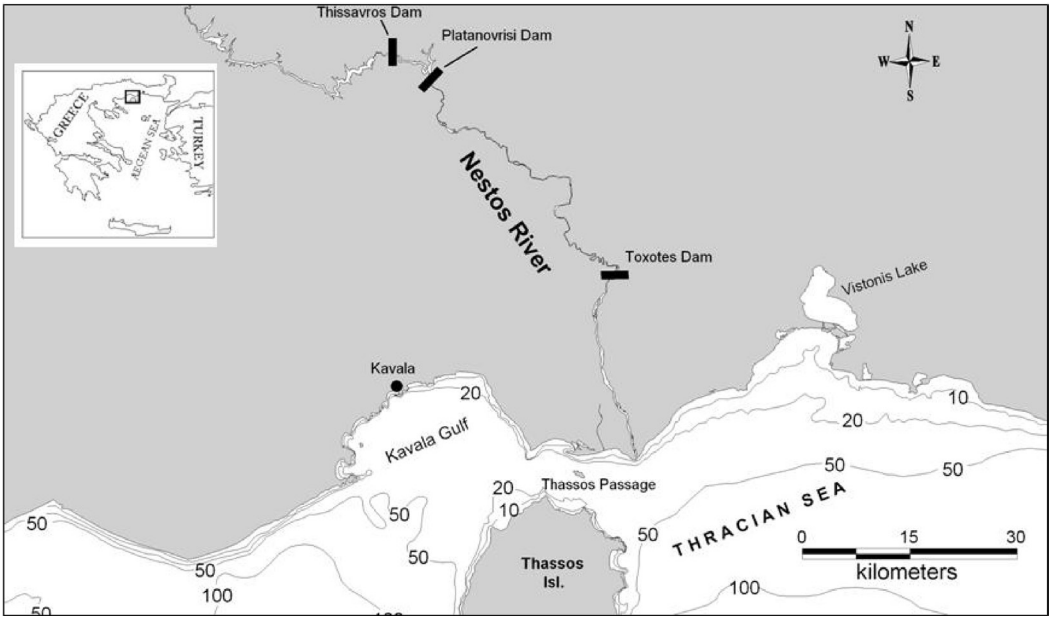

Fig. 1. Map of the Nestos River (Greek part) and its outflow to the Thracian Sea.

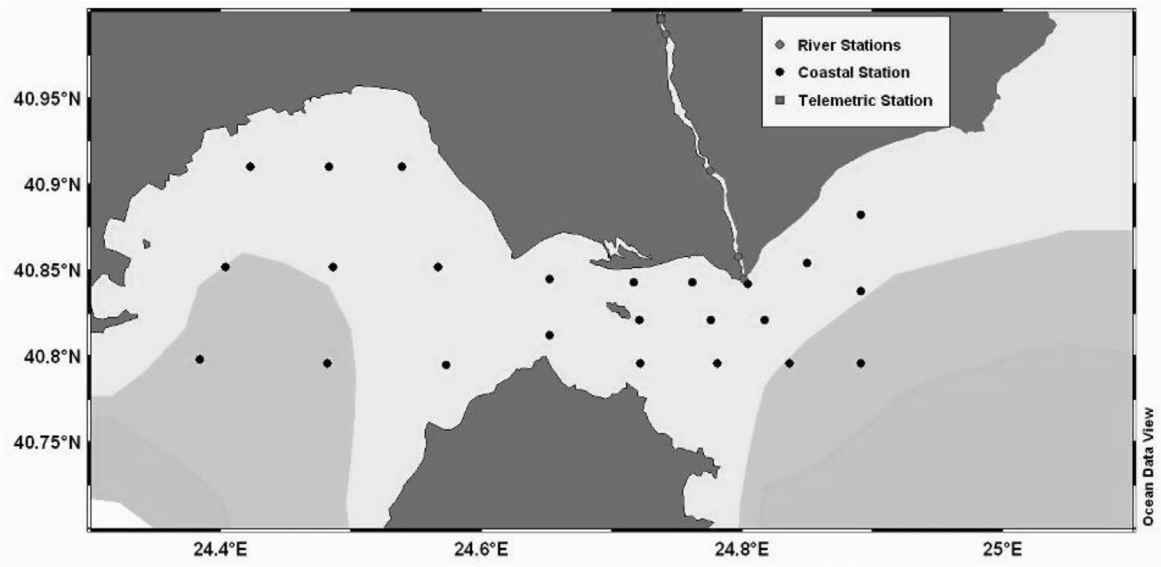

Fig. 2. Map of coastal sampling stations along the Nestos River and coastal zone. The map also shows the location of the automated telemetric station.

station is equipped with an acoustic current-meter and stage sensor, and water discharge occurred through direct measurements at its cross-section and the development of stage-discharge relation. The station is also equipped with a conductivity and temperature meter. Measurements were recorded at a 1-h interval. The above data were used as inputs to the coastal numerical model, in the form of river discharge time-series (Fig. 3). It occurs that year 2006 may be characterised as a 'wet year' in terms of freshwater discharge, since the wet-to-dry mean seasonal discharge equals to 2.02. Higher mean monthly flows were measured in January (135 m^3/s), February (128 m^3/s) and March (118 m^3/s), while the lowest appeared in the summer (June–August), varying between 25.3 and 30.3 m^3/s.

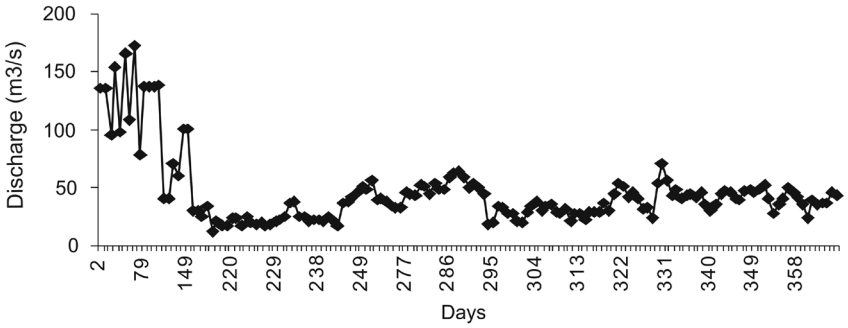

Fig. 3. Nestos River discharge measured from field campaigns and the automated station throughout the year 2006.

2.2.2. Nestos River plume monitoring

One oceanographic survey was conducted in 19 stations of the coastal zone in November 2005. Temperature salinity and conductivity were measured throughout the entire water column and used as initial conditions for the numerical model. Furthermore, three surveys were carried out during high (28/3/2006), moderately high (25/5/2006) and low Nestos River flow (2/8/2006) conditions, in order to test model performance. Temperature, salinity, density and conductivity were measured in the entire water column of the 24 stations, using a Seabird SBE 19plus CTD (Fig. 2). Tidal elevation and three-dimensional velocity vectors throughout the water column were collected using an upward facing 300 KHz ADCP, deployed 15 km west of the river mouth.

2.3. ELCOM model

2.3.1. Model description

Estuary and Lake Computer Model (ELCOM) is a three-dimensional hydrodynamic model developed by the Centre for Water Research (CWR) [25,26]. ELCOM is used to simulate the variation of salinity and temperature in space and time for estuaries, lakes and reservoirs by solving the unsteady, 3D-Reynolds averaged, hydrostatic, Navier–Stokes, Bussinesq equations and the scalar transport equations for salinity, temperature, tracers and incorporating a mixing model for vertical turbulent transport [27]. The unsteady Reynolds-averaged equations were solved on an Arakawa C-grid using a semi-implicit method with quadratic Euler–Lagrange discretization of momentum advection [28], while a conservative ULTIMATE QUICKEST approach was used for scalar transport [29]. Heat exchange through the water surface is governed by standard bulk transfer models found in the literature [30,31]. The principal equations implemented by ELCOM are:

The continuity equation:

$$\frac{\partial U_j}{\partial x_j} = 0 \tag{1}$$

The momentum equation:

$$\frac{\partial U_a}{\partial t} + U_j \frac{\partial U_a}{\partial x_j} = -g\left\{\frac{\partial \eta}{\partial x_a} + \frac{1}{\rho_0}\frac{\partial}{\partial x_a}\int_{z'}^{\eta} \rho' dz\right\} + \frac{\partial}{\partial x_1}\left(v_1 \frac{\partial U_a}{\partial x_1}\right) + \frac{\partial}{\partial x_2}\left(v_2 \frac{\partial U_a}{\partial x_2}\right) + \frac{\partial}{\partial x_3}\left(v_3 \frac{\partial U_a}{\partial x_3}\right) - \in_{a\beta} f U_\beta \tag{2}$$

The vertically-integrated continuity equation:

$$\frac{\partial \eta}{\partial t} = -\frac{\partial}{\partial x_a}\int_b^{\eta} U_a dz \tag{3}$$

The transport equation:

$$\frac{\partial C}{\partial t} + \frac{\partial}{\partial x_j}\left(C U_j\right) = \frac{\partial}{\partial x_1}\left(k_1 \frac{\partial C}{\partial x_1}\right) + \frac{\partial}{\partial x_2}\left(k_2 \frac{\partial C}{\partial x_2}\right) + \frac{\partial}{\partial x_3}\left(k_3 \frac{\partial C}{\partial x_3}\right) + S \tag{4}$$

where j = 1,2,3 represent the three space components, α, β (=1, 2) the two horizontal space components, U the Reynolds-averaged velocity, η the Reynolds-averaged free-surface elevation, ϱo the reference density, ϱ' the in-situ density anomaly, f the Coriolis constant, v_j the eddy viscosity coefficient, k_j the eddy diffusivity coefficient, C the scalar tensor, S the scalar source term. Horizontal eddy diffusivity coefficients are generally assumed similar for both salinity and water temperature [32]. Vertical eddy diffusion was derived from mixing energy budgets used in 1D lake modelling [31]. The S term is representing the heat input/loss from the sea surface for the temperature calculation and evaporation/precipitation at the sea surface and freshwater inputs from point sources regarding salinity calculation.

The boundary conditions at the sea surface due to the wind action are described by the wind stress equations for x_1, x_2 and x_3 direction respectively:

$$(u_*)_\alpha^2 = C_{10}\frac{\rho_{air}}{\rho_{water}}(W_\beta W_\beta)^{1/2} W_\alpha \quad (5)$$

where $(u_*)_\alpha$ is the wind shear velocity in α direction, W_β is the vector wind speed in β direction, and C_{10} is the bulk wind stress coefficient for wind values at 10 m from sea surface.

ELCOM numerical method uses and extend the TRIM scheme [28] by including a hybrid advection scheme for momentum, an energy-based mixing model for vertical diffusion and the conservative advection of scalars using a third-order explicit scheme. Vertical layers are of variable thickness, providing the greatest resolution in the mixing zones.

2.3.2. Model implementation

The modelled area covered the broader Nestos River shelf, discretized into a uniform horizontal grid consisting of 1 × 1 km orthogonal cells, thus including overall 4,717 horizontal cells (Fig. 4). The water column depth at each cell was determined using the 1:50,000 bathymetric chart. A maximum number of 59 variable in thickness layers were used to discretise the water column in each horizontal cell. The water depth in the study area varied between 2 near the coast and 300 m south of the Thassos Island. Surface layers were thinner (0.2 m), with thickness increasing gradually towards the bottom layers, reaching 22 m. Initial conditions in terms of salinity were defined at the grid domain based on the November 2005 survey. Model boundary conditions involved hydrologic, meteorological and tidal forcing. Hydrologic forcing was determined on a daily basis by interpolating the Nestos River discharge measurements, obtained at the Nestos River mouth. For the period that telemetric data were available (August – December 2006), boundary forcing involved the daily averaging of hourly river discharge data. Meteorologic forcing included the synoptic daily datasets of solar radiation intensity, atmospheric temperature, atmospheric relative humidity, precipitation and wind speed and direction acquired from NOAA database (http://ready.arl.noaa.gov/READYamet.php). Tidal forcing at the open boundaries was determined by performing harmonic analysis on the ADCP tidal records, and selecting the basic semi-diurnal M_2 and diurnal S_1 tidal constituents, with amplitudes 0.20 and 0.15 m and phases 32.9 and 350.5 degrees, respectively [33]. The temporal variability of model boundary conditions for the year 2006 is shown in Fig. 5. The time series of salinity at the eastern boundary for the entire year was obtained

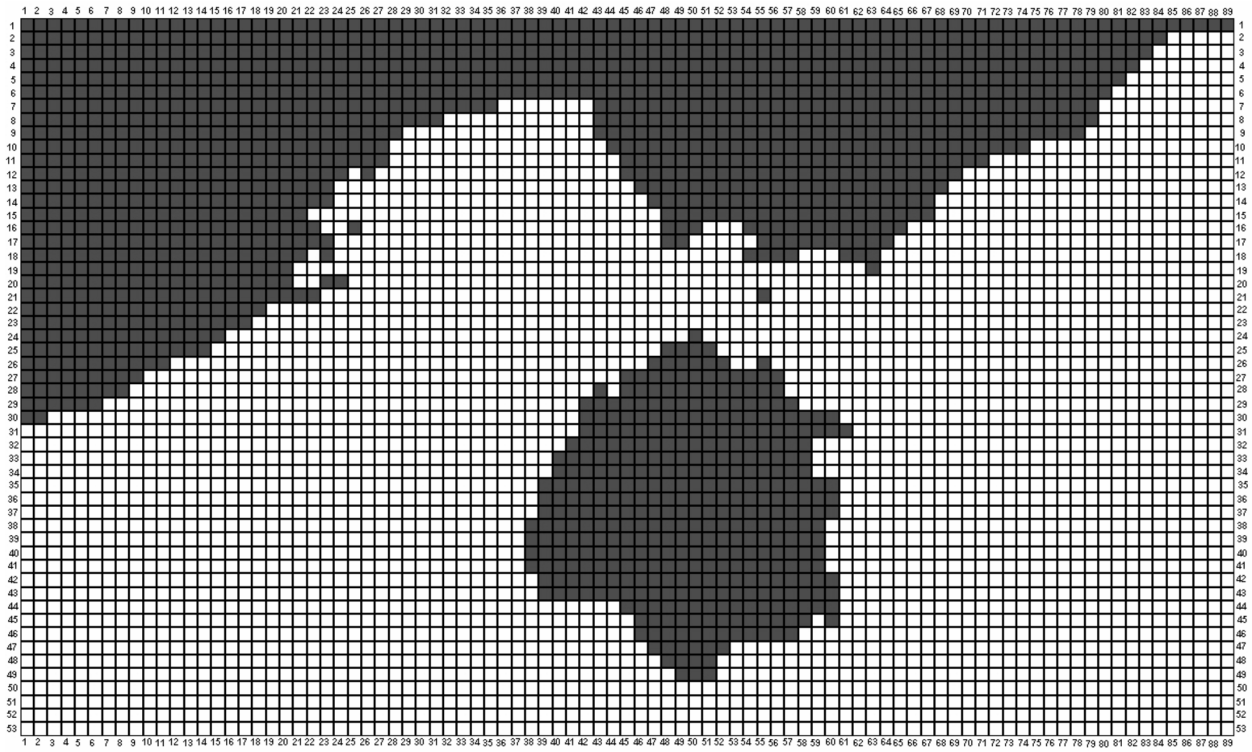

Fig. 4. The computational grid of ELCOM model.

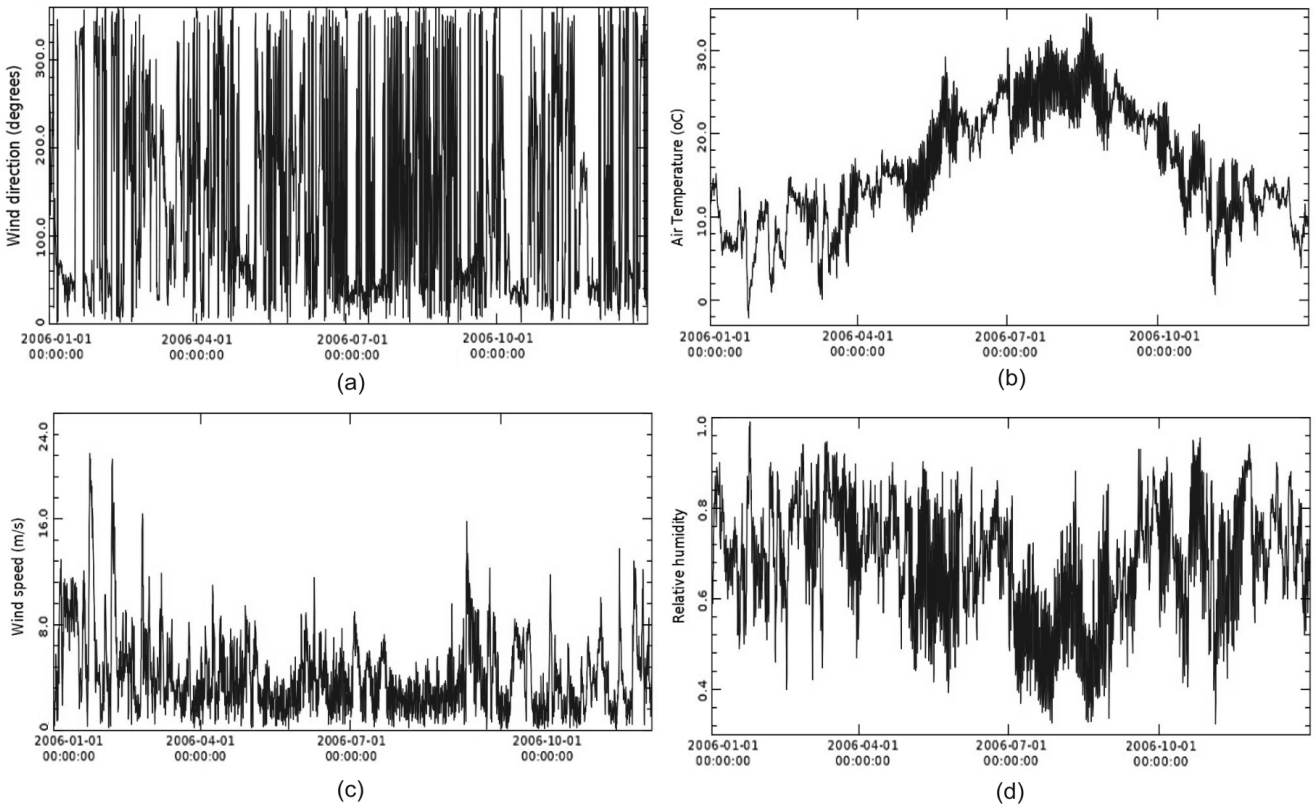

Fig. 5. Model boundary conditions: (a) wind direction, (b) air temperature, (c) wind speed and (d) relative humidity.

by a significant number of field campaigns held in the Thracian Sea. In this way the seasonal variability of the Black Sea water impact which denoted by many authors [21,23,34] is applied to the model (Fig. 6).

2.3.3. Model calibration

The calibration procedure included model runs under several combinations of bottom drag coefficient (C_D) and horizontal eddy diffusivity values ($k_{1,2}$), in order to achieve the best possible salinity simulation. The validity of model calibration was statistically tested in the entire water column ($N = 225$ cases) for a high river flow incident (March 2006), under which the river plume was more evident. The validity of each model output was tested using various statistical tests, such as:

(a) the slope (γ) of the linear regression $P = \gamma M$ between the measured (M) and predicted data (P):

$$\gamma = \frac{\sum_{i=1}^{N}(x_i - \overline{x})(y_i - \overline{y})}{\sum_{i=1}^{N}(x_i - \overline{x})^2} \quad (6)$$

where x_i the measured data, y_i the modeled data and $\overline{x}, \overline{y}$ are the means of measured and modeled values, respectively. When $\gamma > 1$ the model overestimates the observed data, while when $\gamma < 1$ the model underestimates the measured values.

(b) the squared correlation coefficient (R^2), representing the scatter rate between the measured and modeled data from the best fit line:

$$R^2 = \frac{\left[N\left(\sum_{i=1}^{N} x_i y_i\right) - \left(\sum_{i=1}^{N} x_i\right)\left(\sum_{i=1}^{N} y_i\right)\right]^2}{\left[N\left(\sum_{i=1}^{N} x_i^2\right) - \left(\sum_{i=1}^{N} x_i\right)^2\right]\left[N\left(\sum_{i=1}^{N} y_i^2\right) - \left(\sum_{i=1}^{N} y_i\right)^2\right]} \quad (7)$$

where N is the number of observations. Best value for R^2 is unity, at which the measured and modeled values are not scattered around the best fit line for the equation $y = \gamma x$.

(c) the root mean square error (RMSE) and the scatter index (SI). Both parameters have to be close to zero for best model accuracy. The RMSE value derived from the equation:

$$\mathrm{RMSE} = \sqrt{\left[\frac{\sum_{i=1}^{N}(y_i - x_i)^2}{N}\right]} \quad (8)$$

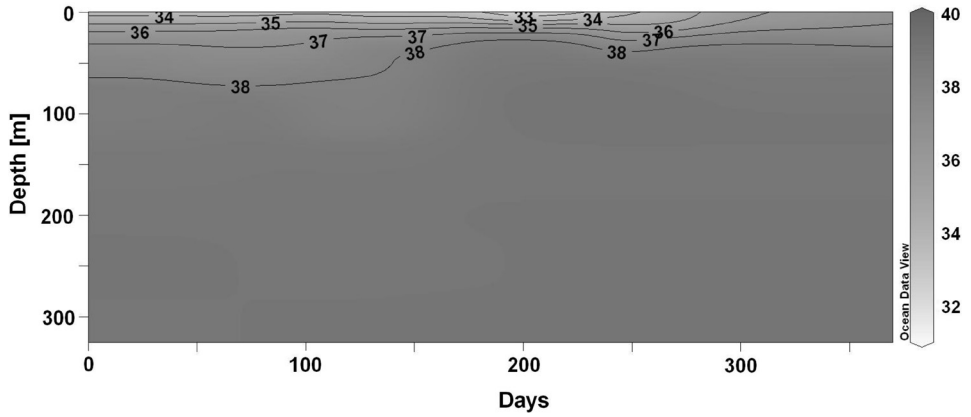

Fig. 6. Time-series of salinity applied in the entire water column of the eastern open boundary. The image also shows the stronger Black Sea water influence during summer.

while the SI is defined as the ratio of RMSE to the average observed value [35]:

$$\mathrm{SI} = \frac{\mathrm{RMSE}}{\bar{x}} \times 100 \quad (9)$$

Lower values of SI indicate less residual variances.

The calibration results for March 2006 showed a good agreement with the measured data for all the combinations of $k_{1,2}$ and C_D parameters (Table 1). The model slightly overestimates the salinity values for all the examined cases, while the R^2 showed very good results and varied between 0.837 and 0.888, thus there was limited scattering. To proceed with model validation, the pair of $C_D = 0.005$ and $k_{1,2} = 0.6$ m^2/s was selected, since it combines the best RMSE and SI values (1.061 and 3.00, respectively) together with sufficient R^2 and γ results. According to [36] and [37], the suggested values are more than sufficient in order to characterize the simulation as successful.

3. Results

3.1. Model validation

In March and under high river discharge (137 m^3/s), the plume covered the entire surface layer of the investigated area (Fig. 7a). However, during the sampling date (28/3/2006), the plume moved northeast of the river mouth, under the influence of low to moderate SSE–SSW winds (0.2–3.4 m/s) lasting for 24 h prior to field campaign. Surface salinity close to the river mouth was measured between 24 and 30 and appeared adequately simulated by the model (27.5–30.8; Fig. 7a). The plume also expanded southwards (29.1–29.9) and westwards (28.8–29.1), reaching the entrance of the Kavala Gulf. The model showed that the southern plume expansion exceeded the sampling region, reaching a distance of 19 km from the river mouth. The western plume expansion was modeled satisfactorily, with surface salinity ranging between 28 inside the Thassos Passage and 32 at the Kavala Gulf entrance. Inside the Kavala Gulf surface salinity was slightly affected by the Nestos River plume.

In May, and under moderately high river flow (101 m^3/s), a well defined plume was formed, expanding westwards under the persistent low magnitude easterly–northeasterly winds (~2 m/s). The plume entered the Kavala Gulf having a sharp frontal form, as shown in Fig. 7b. Lower salinity was measured between 28.9 and 29.7, close to the river mouth, gradually increasing to 31.3 inside the Gulf. The plume expansion to the east and south direction appeared smaller. The plume shape and direction were successfully modeled by ELCOM as shown in Fig. 7b. The model revealed that the plume moved towards the Kavala Gulf with surface velocity of 0.36 m/s at the Thassos Passage. When in the Passage, the plume was pressed inshore due to Ekman drift producing calculated surface salinity values between 29.3 and 31.6. As a result, the model was unable to predict the smaller plume expansion to the east and south of the estuary, resulting to relatively increased salinity within 2 km from the mouth (34.6–35.4). As a result, the comparison between measured and calculated salinities showed lower but still significant correlation ($N = 337$, $R^2 = 0.64$, $\gamma = 1.04$, RMSE = 2.16, SI = 6.2%).

In August, Nestos plume is restricted at a close distance from the river mouth due to low freshwater discharge (15.8 m^3/s; Fig. 7c). In this area, the salinity was measured between 31.5 and 32.3. The model predicted similar salinity range (31.5–33.7), but simulated even lower salinity at the small embayment to the west of the river mouth and close to the coastline (26.7). It seems that the SE wind blowing for 12 h with an average speed of 2.3 m/s, dragged and trapped the plume inside this small gulf. This time the plume did not reach the entrance of the Kavala Gulf, due to the extremely limited river flow. The

Table 1
Model simulation performance for salinity during March 2006, under different drag coefficients and eddy diffusivities values

		Salinity			
	$k_{1,2}$ (m_2/s)	R^2	γ	RMSE	SI (%)
C_D = 0.001	0.2	0.873	1.012	1.225	3.574
	0.4	0.845	1.017	1.357	3.959
	0.6	0.859	1.011	1.158	3.376
C_D = 0.003	0	0.874	1.012	1.092	3.185
	0.2	0.885	1.012	1.052	3.067
	0.4	0.885	1.013	1.077	3.141
	0.6	0.888	1.015	1.092	3.184
	0.8	0.883	1.015	1.120	3.267
C_D = 0.005	0	0.877	1.013	1.098	3.203
	0.1	0.878	1.012	1.077	3.141
	0.2	0.883	1.014	1.103	3.216
	0.4	0.885	1.012	1.072	3.127
	0.5	0.883	1.014	1.096	3.197
	0.6	0.886	1.011	1.061	3.000
	0.8	0.888	1.014	1.077	3.141
	1.0	0.875	1.015	1.135	3.312
	2.0	0.837	1.015	1.131	3.300
	3.0	0.886	1.013	1.075	3.138

comparison between measured and computed salinities presented very good values for all statistical parameters (N = 230, R^2 = 0.80, γ = 1.05, RMSE = 2.31, SI = 6.6%). The scatter diagrams between the measured and simulated salinity for all the examined cases are presented in Fig. 8.

After the successful model validation, the general behaviour of the Nestos River plume was described under variable river discharge and wind conditions. Under Model Run 1 the plume response was examined under conditions of elevated river discharge (~100 m^3/s) and the influence of E–NE winds of moderate magnitude (2–5 m/s); under Model Run 2 the plume expansion is described under W–NW winds (~3.5 m/s) and high river flow (~130 m^3/s). Model Runs 3 and 4 illustrate the plume behaviour for low Nestos flows (~25 m^3/s), under E–NE and SW–W winds, respectively.

3.2. Model Run 1 — high river discharge and E–NE winds

This case simulates the conditions of 23/2/2006, characterised by easterly-to-north-easterly winds influencing continuously the area for approximately 12 h with an average speed of 3.4 m/s (1.9–5.3 m/s). Nestos River flow at this period was above the annual average, oscillating around 100 m^3/s. Model results illustrated that the plume directed westwards and entered Thassos passage with a surface flow of 0.3–0.6 m/s. The plume was confined close to the northern coastline and entered the Kavala Gulf (Fig. 9a). In the Kavala Gulf, the plume retained a NW flow, moving almost parallel to the coastline, while at the same time preserving its momentum, having an average surface speed of 0.44 m/s. Water salinity 1 km from the river mouth was found at 25.7, increasing gradually to 32.8 inside the Thassos passage and reaching 33.1–34.3 inside the Kavala Gulf. Under these conditions, plume expansion towards the east of the river mouth was negligible, since salinity increases rapidly to 35.7 at close distance from the mouth. Some plume parcels simulated south of the mouth are attributed to western wind action, occurred during 21/2/2006 (Fig. 10a).

3.3. Model Run 2 – high river discharge and W–NW winds

This case simulates the conditions of 18/1/2006 under the prevalence of W–NW winds, with average magnitude of 3.5 m/s and duration of 27 h. The plume marked mainly a southern expansion, due to the high river discharge (130 m^3/s), obtaining a mean velocity of 0.21 m/s. Plume salinity ranged between 25 at the river mouth and 34.8 at the eastern coast of Thassos (Fig. 9b). The plume front was simulated 16 km south of the river mouth. Inside Thassos passage salinity was modelled at elevated values, varying between 35.6 and 36.3. However, inside the Kavala Gulf surface salinity was simulated at lower levels with

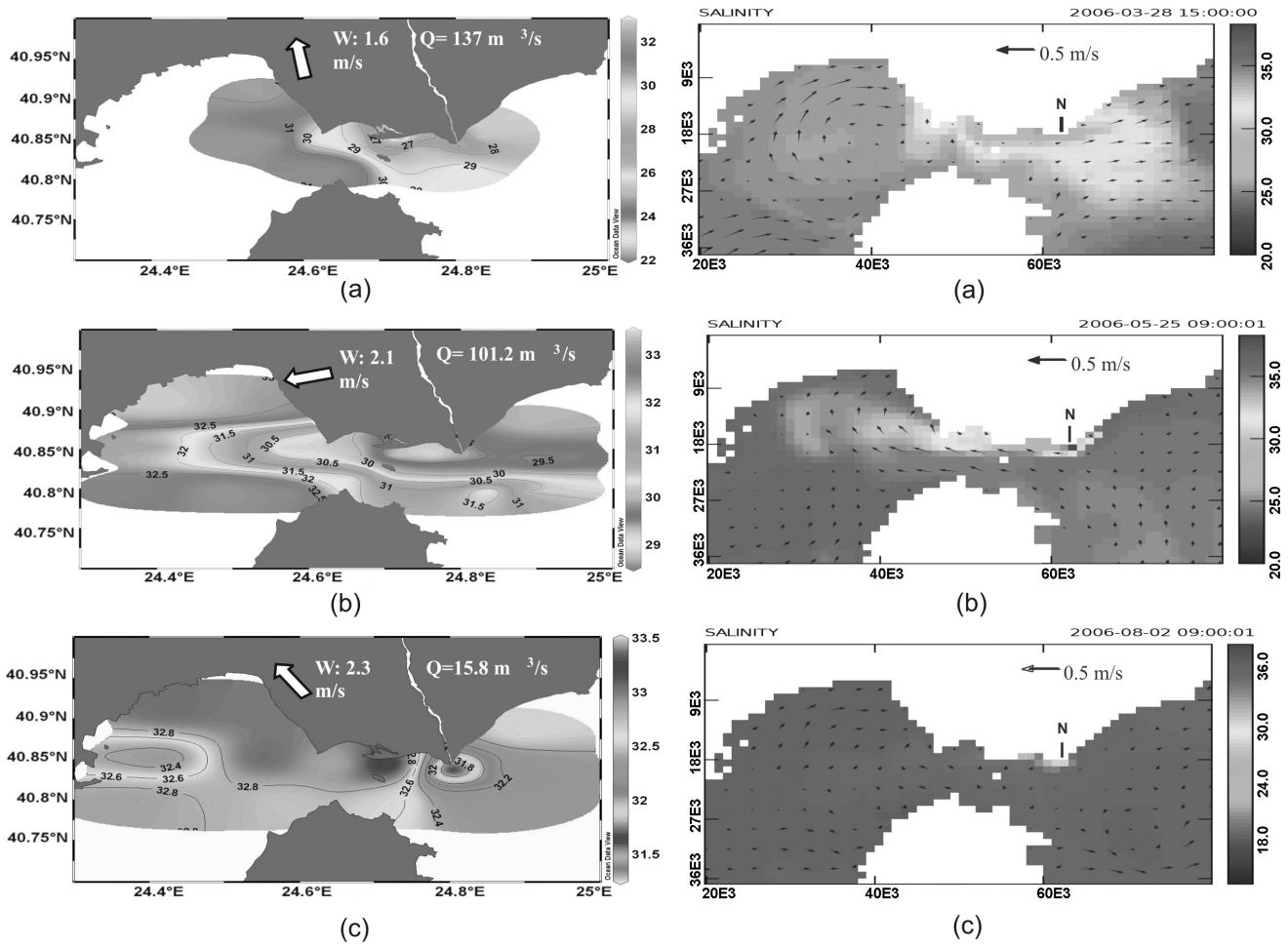

Fig. 7. Surface salinity distribution of observed (left panel) and predicted values (right panel) for: (a) March, (b) May and (c) August 2006. At the left panel the daily median wind direction and the weekly averaged discharge are also presented.

an average value of 34.9. The plume travelled towards west due to prolonged E-NE winds, blowing from 12/1 to 16/1 (Fig. 10b).

3.4. Model Run 3 – low river discharge and E–NE winds

In June (12/6/2006), Nestos River discharge was fairly low, reaching 29.8 m^3/s, a typical flow for this season. East-to-north-east winds prevailed in the area for a period of 21 h, having an average wind speed of 3.2 m/s. As it can be seen in Fig. 9c, the plume was confined at a very close distance from the river mouth and bended slightly rightwards. The salinity 1 km from the mouth was simulated at 31.9, increasing rapidly to 35.3 within 1 km southwards. Based on the model results, it occurs that the plume covered an area of approximately 18 km^2. Lower salinity was simulated at the small gulf located west of the river mouth (S = 30), receiving freshwater from the Nestos River and a drainage ditch. Surface velocity within the plume was simulated between 0.09 m/s inside the small gulf and 0.36 m/s 2 km west of the mouth. The model also showed that no expansion occurred to the west of the river mouth.

3.5. Model Run 4 – low river discharge and W–SW winds

Model Run 4 simulated the conditions of 15/7/2006, when the principal wind component was SW–W with magnitude of 1.1 m/s for a period of 24 h. Nestos River discharge oscillated at low levels, as in Model Run 3 (~25.3 m^3/s). Model results showed that the plume occupied a limited area of the surface layer and was strictly confined in the vicinity of the river mouth (Fig. 9d). No further plume expansion was computed, due to the low river discharge. Salinity in the rest of the investigated area was simulated between 35.9 and 36.7. Water ve-

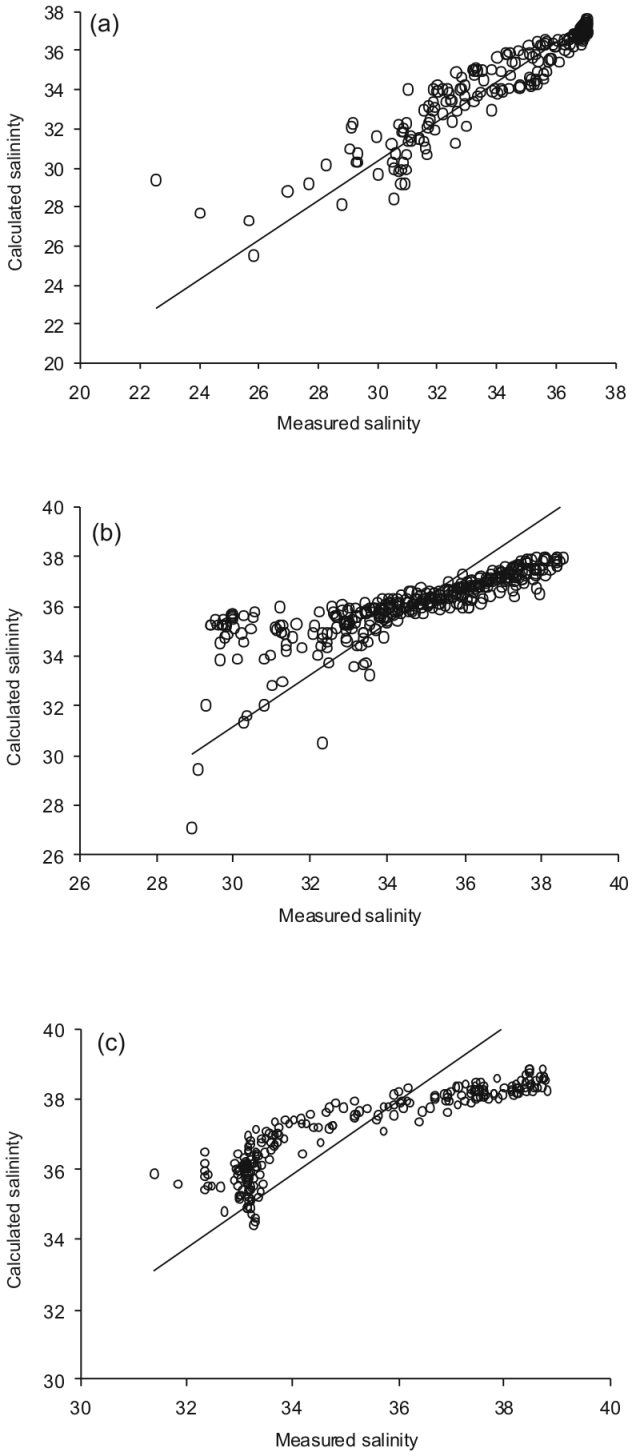

Fig. 8. Correlation of salinity between the calculated and observed data for: (a) March, (b) May and (c) August 2006.

locity within this limited plume was also found weak (0.1–0.3 m/s), analogous to the low wind magnitude and orientated towards the east from the mouth area.

4. Discussion

The plume behaviour under variable river discharge and wind directions was investigated with the use of a numerical model, after successful calibration and validation. The simulation showed that the principal mechanism controlling the plume orientation and expansion from the mouth is the wind. Similar results were denoted by many authors [38,39]. The tidal mechanism plays a minor role in the plume mixing with the ambient water, due to the micro-tidal Mediterranean environment. The wind action is dominant in determining plume behaviour in such systems [40,41]. Moreover, river discharge is essential and provides the adequate momentum to transport the plume at large distances from the river mouth [40]. Under high river discharge and E-NE winds, the plume is directed westwards and is pushed towards the northern coastline as a result of the Ekman drift [42]. River discharge at this particular period is sufficient and with the assistance of favourable winds, the plume is transported approximately 30 km westwards, entering the Kavala Gulf through the Thassos Passage. Coastal morphology plays a significant role to this western expansion. The Thassos Passage created by the existence of the Thassos Island, acts like a funnel providing additional acceleration to the plume. The surface velocity of the plume in this strait was simulated at 0.44 m/s, while outside the passage velocity decreased to 0.2–0.3 m/s. This effect drives the plume at its maximum distance from the river mouth. Coastal morphology plays an important role on the plume deflection, dispersion and preservation and affects its general behaviour [13,43]. Eventually, the plume penetrates the Kavala Gulf and declines to the northwest, following the coastline slope (Fig. 9a). Furthermore, the anticyclonic eddy produced inside the Kavala Gulf in March 2006 (Fig. 7a) preserves and recycles this small plume water mass. This eddy is produced by the combination of westward water circulation, wind variability, bottom topography and coastline morphology generated by the existence of the strait. The Thassos passage can be considered as a source of brackish water with an opening of 7 km, every time persistent eastern wind occurs. As the water travels to the west and exits the Thassos passage, it suddenly becomes an 'offshore current', while at the same time the area gradually deepens gently from 26 m at the source to 42 m in the middle of the gulf. This situation is producing an anticyclonic eddy similar to those reported by many authors [43–45]. However, in terms of water circulation in the examined area, this eddy is restricted within the Kavala Gulf.

Under W–NW winds and high river discharge, the model showed that the plume expanded offshore, driven once again by the Ekman drift [42,46]. This is a common behaviour for a plume produced by adequate river discharge, as pointed out by many authors [47,48]. Despite the higher river discharge the plume formed under Model

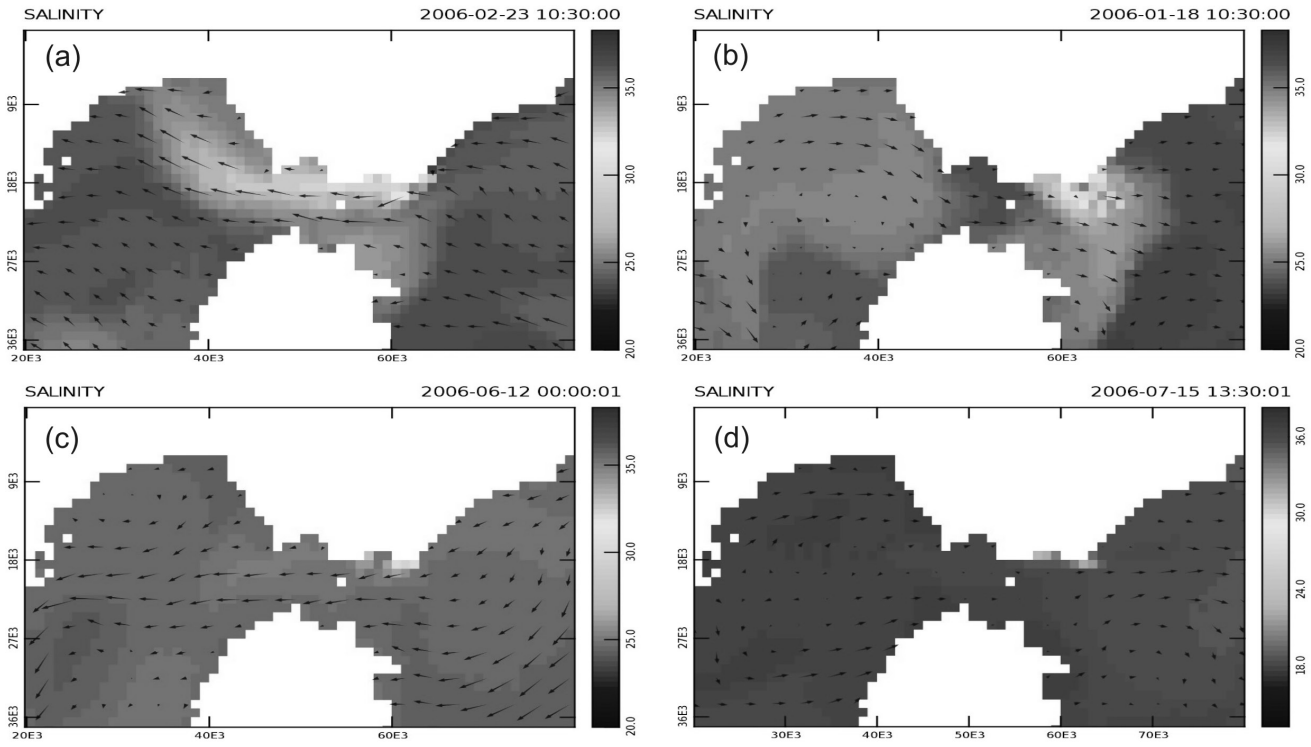

Fig. 9. Plume evolution under (a) Model Run 1, (b) Model Run 2, (c) Model Run 3 and (d) Model Run 4.

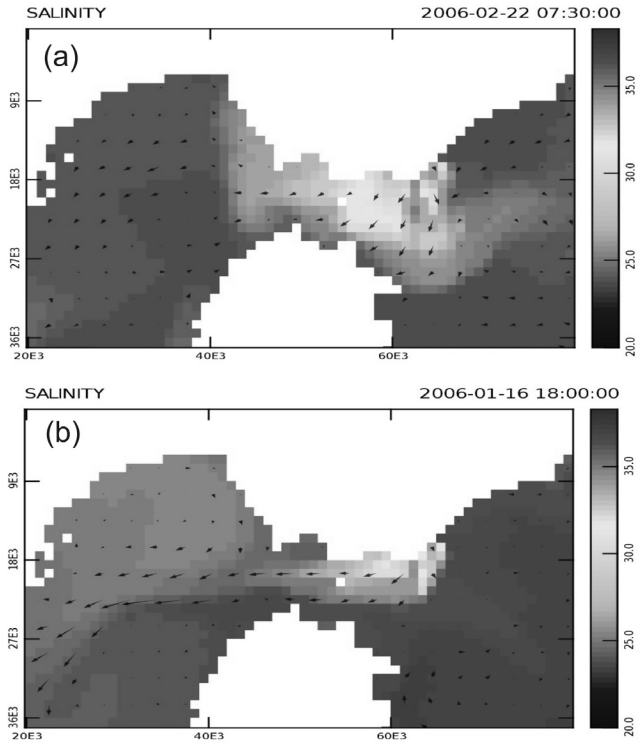

Fig. 10. Plume development (a) on 22/2/2006 and (b) on 16/1/2006.

Run 2 occupied less surface area and appeared generally weaker, compared to that of Model Run 1.

Under the Model Runs 3 and 4, rapid mixing conditions dominated leading to the plume dilution, as a result of limited Nestos River discharge. In this way, the plume is unable to move away from the mouth and appears dispersed immediately by the wind action. The only area which is able to preserve some plume volume is the small gulf located 5 km to the west of the river mouth. This area is less influenced by the wind since it is characterized by low surface velocity (0.09 m/s), while it receives limited freshwater parcels from Nestos River and an existing drainage ditch.

Following the previously presented model results, the temporal variability of salinity and velocity profiles throughout 2006, at a grid cell located inside the Thassos Passage, is shown in Fig. 11. These parameters are daily averaged, thus results are smoothed through two consecutive tidal cycles, in order to diminish the limited, but still evident, tidal impact. It occurs that the Thassos Passage received the stronger plume influence during the winter (January to March) and in May (Fig. 11a). In situations such as January and March, the plume occupied the top 5 m of the water column. These episodes of freshwater arrival are accompanied by the surface layer western movement as presented in Fig. 11b. The presence of the plume inside the passage appeared weaker (32.7–34.8) in

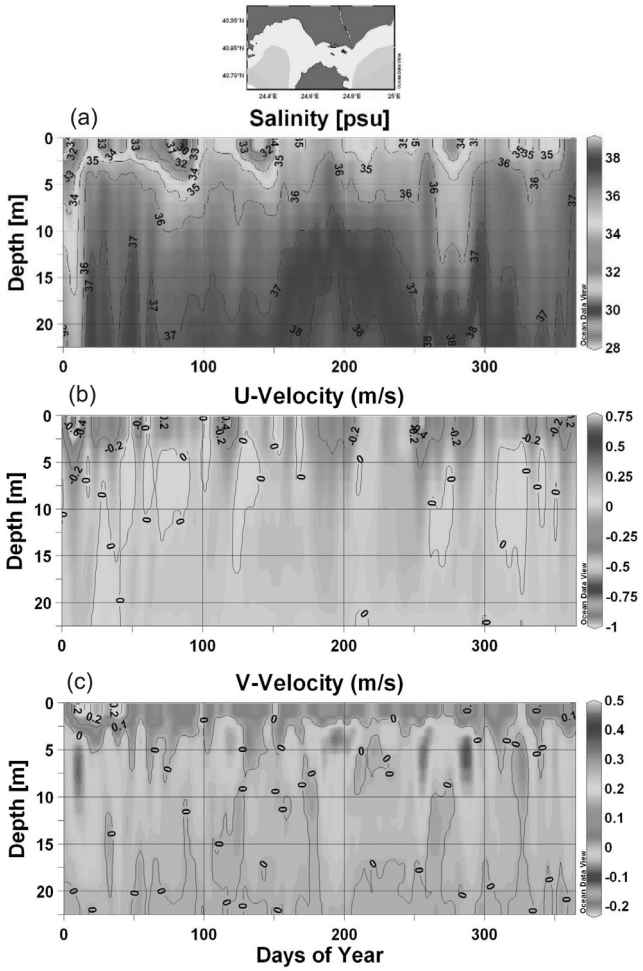

Fig. 11. Vertical distribution of (a) salinity, (b) along-shore velocity and (c) cross-shore velocity for a station located 5 km west of the Nestos River mouth and inside the Thassos Passage. Negative along-shore and cross-shore velocities represent western and northern movement, respectively.

the October–December period (Fig. 11a) due to the lower river discharge (40.8–55 m^3/s). However, in occasions like these, small plume amounts managed to penetrate inside the Kavala Gulf under prolonged low magnitude north-eastern winds (not shown). In fact, the surface layer directed westwards for the majority of the year as a result of two incidents: (i) based on the NOAA recordings the eastern wind and its secondary components (20–150°) were accounted for the 54.9% of the annual wind activity and (ii) the general water circulation of the area is influenced by the BSW which is arriving at the eastern boundary and moving towards west [23,34]. Eastern movement occurred at a percentage of 29% of the year. Highest alongshore velocities were simulated in January (0.5–1.0 m/s) and September (0.4–0.8 m/s; Fig. 11b). This is accounted to the high magnitude of north-eastern winds in January (average: 11.3 m/s; max: 20.9 m/s) and September (average: 8.8 m/s; max: 15.8 m/s), which were blowing continuously for 6 and 5.3 days, respectively (Figs. 5a and 5c). At deeper layers, the alongshore velocity was simulated at lower levels, ranging between 0 and 0.12 m/s.

On the other hand, the cross-shore velocity at the surface layer was simulated at very low levels (average 0.07 m/s), indicating the limited lateral water transport in the Passage (Fig. 11c). High lateral values were computed in January, reaching 0.48 m/s, as a result of the increased magnitude north-eastern winds. It seems that the general circulation of the area favours the southern water transport. However, a counter-current was created below 3 m depth during most of the year, and this northward movement is characterized by reduced velocities (0.01–0.12 m/s).

5. Conclusions

The combination of field observations with numerical modelling, delivered for the first time significant information on the Nestos plume behaviour. The results of the numerical model are in a good agreement with the observed data, thus, we feel confident to predict the expansion of the Nestos plume under variable combinations of river discharge and winds. The presented cases cover nearly 70% of the conditions prevailing in the area throughout year 2006. Results showed that Nestos plume is influenced by a number of external forces and morphological characteristics, but the prevailing force is the wind action. Under eastern winds, the plume is expanding to the west, while western winds can carry the plume offshore. The existence of the Thassos Passage is also important, since it accelerates the westward plume movement. Under low to moderate river flow (40–50 m^3/s), the plume also manages to enter the Kavala Gulf only during extended eastern low magnitude winds (≤ 2.0 m/s). Hydrodynamic models have become an important tool that can be used to reveal the principal mechanisms that influence the plume expansion and the degree of the plume response to these external forces.

References

[1] F. Diaz, J-J. Naudin, C. Courties, P. Rimmelin and L. Oriol, Biogeochemical and ecological functioning of the low-salinity water lenses in the region of the Rhone River freshwater influence, NW Mediterranean Sea. Continent. Shelf Res., 29 (2010) 1397–1409.

[2] C. Narayanan and R. Garvine, Large scale buoyancy driven circulation on the continental shelf. Dynamics Atmospheres Oceans, 36 (2002) 125–152.

[3] J.H. Simpson, Physical processes in the ROFI regime. J. Marine Systems, 12 (1997) 3–15.

[4] J.I. Hedges and R.G. Kiel, Sedimentary organic matter preservation: an assessment and speculative synthesis. Marine Chem., 49 (1995) 81–115.

[5] D. Justic, N.N. Rabalais and R.E.Turner, Stoichiometric nutrient balance and origin of coastal eutrophication. Marine Pollut. Bull., 30 (1995) 41–46.

[6] D. Justic, N.N. Rabalais, R.E. Turner and Q. Dortch, Changes in nutrient structure of river-dominated coastal waters: Stoichiometric nutrient balance and its consequences. Estuarine, Coastal Shelf Sci., 40 (1995) 339–356.
[7] D.P. Hamilton, T. Chan, M.S. Robb, C.B. Pattiaratchi and M. Herzfeld, The hydrology of the upper Swan River Estuary with focus on an artificial destratification trial. Hydrol. Proc., 15 (2001) 2465–2480.
[8] R.E. Turner and N.N. Rabalais, Coastal eutrophication near the Mississippi River Delta. Nature, 368 (1994) 619–621.
[9] K. Yin, X. Song, J. Sun and M.C.S. Wu, Potential P limitation leads to excess N in the Pearl River estuarine costal plume. Continent. Shelf Res., 24 (2004) 1895–1907.
[10] O. Le Pape, F. Chauvet, Y. Desaunnay and D. Guerault, Relationship between interannual variations of the river plume and the extent of nursery grounds for the common sole (*Solea solea*, L,) in Viliaine Bay. Effects on recruitment variability. J. Sea Res., 50 (2003) 177–185.
[11] A.M, Aquilar-Islas and K.W. Bruland, Dissolved manganese and silicic acid in the Columbia River plume: A major source to the California current and coastal waters off Washington and Oregon. Marine Chem., 101 (2006) 233–247.
[12] G. Sylaios, N. Kamidis and V.A. Tsihrintzis, Impact of river damming on coastal stratification–mixing processes: The cases of Strymon and Nestos Rivers, N. Greece. Desalination, 250 (2010) 302–312.
[13] M. Mestres, J.P. Sierra and A. Sanchez-Arcilla, Factors influencing the spreading of a low-discharge river plume. Continent. Shelf Res., 27 (2007) 2116–2134.
[14] J.L. Wellmeyer, M.C. Slattery and J.D. Philips, Quantifying downstream impacts of impoundment on flow regime and channel platform, lower Trinity, Texas. Geomorphol., 69 (2005) 1–13.
[15] F.J. Magilligan and K.H. Nislow, Changes in hydrologic regime by dams. Geomorphol., 71 (2005) 61–78.
[16] A. Wolf, J. Natharius, J. Danielson, B. Ward and J. Pender, International river basins of the 21 world. Intern. J. Wat. Resources Develop., 15 (1999) 387–427.
[17] G. Sylaios and E. Bournaski, The transboundary Nestos/Mesta River: An overview on hydrology and environment. In: P. Economidis, M. Koutrakis, A. Apostolou, M. Vassilev and L. Pehlivanov, Atlas of Nestos River fish fauna, Prefectural Authority of Drama-Kavala-Xanthi Publications, Xanthi 2009, pp. 35–56.
[18] E. Darakas, The transboundary River Nestos and its water quality assessment: cross-border cooperation between Greece and Bulgaria. Environmentalist, 22 (2002) 367–375.
[19] A. Psilovikos, S. Margoni and A. Psilovikos, Simulation and trend analysis of the water quality monitoring daily data in Nestos River Delta. Contribution to the sustainable management and results for the years 2000–2002. Environ. Monitor. Assess., 116 (2006) 543–562.
[20] N.Th. Skoulikidis, The environmental state of rivers in the Balkans – A review within the DPSIR framework. Sci. Total Environ., 407 (2009) 2501–2516.
[21] H. Yüce, Northern Aegean water masses. Estuarine Coastal Shelf Sci., 41 (1995) 325–343.
[22] V. Lykousis, G. Chronis, A. Tselepides, N.B. Price, A. Theocharis, I. Siokou-Frangou, F. Van Wambeke, R. Danovaro, S. Stavrakakis, G. Duineveld, D. Georgopoulos, L. Ignatiades, A. Souvermezoglou and F. Voutsinou-Taliadouri, Major outputs of the recent multidisciplinary biochemical researches undertaken in the Aegean Sea. J. Marine Systems, 33–34 (2002) 313–334.
[23] G. Sylaios, N. Stamatis, A. Kallianiotis and P. Vidoris, Monitoring and assessment of land-based nutrient loadings, distributions and cycling within Kavala Gulf. Wat. Resources Manage., 19 (2005) 713–735.
[24] S.E. Poulos, P.G. Drakopoulos and M.B. Collins, Seasonal variability in sea surface oceanographic conditions in the Aegean Sea (Eastern Mediterranean): an overview. J. Marine Systems, 13 (1997) 242–244.
[25] B.R. Hodges, Numerical Techniques in CWR-ELCOM (Code Release v.1). CWR Manuscript WP1422 BH, Centre for Water Research, University of Western Australia Publications, Perth, 2000.
[26] B. Hodges and C. Dallimore, Estuary and Lake Computer Model: ELCOM Science Manual Code Version 2.0.0. Centre for Water Research, University of Western Australia Publications, Perth, 2001.
[27] B. Laval, J. Imberger, B.R. Hodges and R. Stocker, Modeling circulation in lakes: spatial and temporal variations. Limnol. Oceanography, 48 (2003) 983–994.
[28] V. Casulli and R.T. Cheng, Semi-implicit finite difference methods for three dimensional shallow water flow. Intern. J. Numerical Methods in Fluids, 15 (1992) 629–648.
[29] B.P. Leonard, The ultimate conservative difference scheme applied to unsteady one-dimensional advection. Computer Methods Appl. Mech.l Eng., 88 (1991) 17–74.
[30] J. Amorocho and J.J. Devries, A new evaluation of the wind stress coefficient over water surfaces. J. Geophys. Res., 85 (1980) 433–442.
[31] J. Imberger and J.C. Patterson, A dynamic reservoir simulation model—DYRESM 5. In: H. Fisher, Transport Models for Inland and Coastal Waters, Proc. Symposium on Predictive Ability. Academic Press, New York, 1981, pp. 310–361.
[32] C. Pattiaratchi, J. Newgard and B. Hollings, Physical oceanographic studies of Adelaide coastal waters using high resolution modeling, in-situ observations and satellite techniques-Sub Task 2 Final Technical Report. ACWS Technical Report No. 20 prepared for the Adelaide Coastal Water Study Steering Committee. School of Environmental Systems Engineering, University of Western Australia, 2007.
[33] G.K. Sylaios, C. Akratos, V. Pissinaras, N. Kamidis and V.A. Tsihrintzis, 'TRITON': A monitoring station for wave climate, hydrodynamics and turbidity offshore Nestos River mouth, N. Greece. In: Proc. 9th International Conference on Protection and Restoration of the Environment, Kefalonia, 2008.
[34] V.H. Kourafalou and K. Barbopoulos, High resolution simulations on the North Aegean Sea seasonal circulation. Annales Geophys., 21 (2003) 251–265.
[35] C.S. Akratos, J.N.E. Papaspyros and V.A. Tsihrintzis, Artificial neural network use in ortho-phosphate and total phosphorus removal prediction in horizontal subsurface flow constructed wetlands. Biosyst. Eng., 102 (2009) 190–201.
[36] R.C. Ris, L.H. Holthuijsen and N. Booij, A third generation wave model for coastal regions. 2: Verification. J. Geophys. Res., 104 (1999) 7667–7681.
[37] O. Makarynskyy, D. Makarynska, M. Kuhn and W.E. Featherstone, Predicting sea level variation with artificial neural networks at Hillarys Boat Harbour, Eastern Australia. Estuarine Coastal Shelf Sci., 61 (2004) 351–360.
[38] L. Ferrer, A. Fontán, J. Mader, G. Chust, M. González, V. Valencia, A. Uriarte and M.B. Collins, Low salinity plumes in the oceanic region of the Basque Country. Continent. Shelf Res., 29 (2009) 970–984.
[39] W.-C. Liu, W.-B. Chen, R.T. Cheng and M.-H. Hsu, Modelling the impact of wind stress and river discharge on Danshuei River plume. Appl. Math. Model., 32 (2008) 1255–1280.
[40] M. Mestres, J.P. Sierra, A. Sánchez-Arcilla, J.G. Del Rio, T. Wolf, A. Rodríguez and S. Oillon, Modelling the Ebro River plume. Validation with field observations. Sci. Marina, 67 (2003) 379–391.
[41] C. Ulses, C. Grenz, P. Marsaleix, E. Schaaff, C. Estournel, S. Meulé and C. Pinazo, Circulation in a semi-enclosed bay under influence of strong freshwater input. J. Marine Syst., 56 (2005) 113–132.
[42] S.Y. Chao, River forced estuarine plumes. J. Phys. Oceanography, 18 (1988) 72–88.
[43] V.H. Kourafalou, River plume development in semi-enclosed Mediterranean regions: North Adriatic Sea and Northwestern Aegean Sea. J. Marine Syst, 30 (2001) 181–205.
[44] K. Tanaka, Y. Mishida, T. Komatsu and K. Ishigami, Spreading of river water in Suruga Bay. J. Oceanography, 65 (2009) 165–177.
[45] L. Wang and D. Justić, A modeling study of the physical pro-

cesses affecting the development of seasonal hypoxia over the inner Luisiana-Texas shelf: Circulation and stratification. Continent. Shelf Res., 29 (2009) 1464–1476.
[46] D. Shankar, P.N. Vinayachandran and A.S. Unnikrishnan, The monsoon currents in the North Indian Ocean. Progress Oceanography, 52 (2002) 63–120.
[47] B. Hickey, S. Geier, N. Kachel and A. MacFadyen, A bi-directional river plume: The Columbia in summer. Continent. Shelf Res., 25 (2005) 1631–1656.
[48] P. MacCready, N.S. Banas, B.M. Hickey, E.P. Dever and Y. Liu, A model study of tide- and wind-induced mixing in the Columbia River Estuary and plume. Continent. Shelf Res., 29 (2009) 278–291.